

Received March 3, 2020, accepted March 12, 2020, date of publication March 17, 2020, date of current version April 2, 2020.

Digital Object Identifier 10.1109/ACCESS.2020.2981444

An Adaptive D-FACTS for Power Quality Enhancement in an Isolated Microgrid

AHMED HUSSAIN ELMETWALY¹, AZZA AHMED ELDESOUKY²,
AND ABDELHAY AHMED SALLAM², (Life Senior Member, IEEE)

¹Higher Institute of Engineering, Elshorouk Academy, Cairo 41511, Egypt

²Department of Electrical Power Engineering, Port Said University, Port Fouad 42526, Egypt

Corresponding author: Ahmed Hussain Elmetwaly (eng.ahmedhussain7@gmail.com)


ABSTRACT Technologies of microgrids (MGs) help power grid evolve into one that is more efficient, less polluting, reduced losses, and more flexible to provide energy consumers' want and need. Because of the nature of various renewable energy sources (RESs) integrated into the MGs such as variability and inability to accurately predict and control, different technical problems are created. Power quality is one of the most important issues to be addressed, especially harmonic distortion and voltage stabilization. Many devices have been proposed to improve these two aspects that may result from loads nonlinearity and sources uncertainty. In this study, an adaptive switched filter compensator (ASFC) with developed proportional-integral-derivative (PID) controller is proposed to improve the overall dynamic performance of the MGs. The PID's controller gains are optimally tuned via the application of grasshopper's optimization algorithm (GOA) to act adaptively with self-tuning as the operating conditions may subject to change during MG operation. Different case studies are proposed to reveal the robustness of the presented ASFC on harmonic mitigation, dynamic voltage stabilization, reactive power compensation and power factor improvement considering the features of RESs such as variations of wind speed, solar PV irradiation and temporary fault conditions. A distribution synchronous static compensator (D-STATCOM), as one of the most popular D-FACTS, with optimal tuned PID controller by using the GOA is also proposed. To validate both the proposed ASFC topology and the modified D-STATCOM, comparative studies including what has been published in literature are examined by using MATLAB/Simulink platform. The results advocate the effectiveness, robustness and latency of the proposed devices.

INDEX TERMS Microgrids (MGs), adaptive switched filter capacitor (ASFC), distribution synchronous static compensator (D-STATCOM), distribution flexible alternative current transmission system (D-FACTS), power quality (PQ), grasshopper's optimization algorithm (GOA), PID Controller.

I. INTRODUCTION

Integration of distributed energy resources (DERs), renewables and non-renewables, forming what is called 'microgrids (MGs)' has been widely deployed to benefit both utilities and consumers. MGs are continuously developed along with the progress in information and communication technologies (ICTs).

Three modes of operation MGs can operate in; utility grid-connected, islanded and isolated. In addition, MG control strategies can be categorized into three levels; (i) primary control, which is a local control for each load and each resource

The associate editor coordinating the review of this manuscript and approving it for publication was Shiwei Xia .

in the MG. It is based on the local measurements of the parameters necessary for managing and controlling the MG, (ii) secondary control that is responsible for MG operation according to the mode of operation used, and (iii) tertiary control, which is the highest level of control. It coordinates multiple MGs interacting with one another in the system and communicates requirements from the utility grid [1].

Therefore, primary and secondary controls are associated with the MG operation itself, whereas the tertiary control is considered as part of the utility grid. Regardless of the kind of operation mode, MG components should be interoperable and with interfaces complying with functional standards defined by the MGs as well as the controller should enable the MGs to manage themselves and operate autonomously.

Renewable energy sources (RESs) are nowadays encouraged by utility companies to be integrated into the MG. Because of the nature of various renewable sources (e.g., wind and solar PV) such as variability and inability to accurately predict and control, different technical problems are created. A tremendous amount of research in addition to attention of power system planners and operators are taken place in providing the consumers with electrical energy as economically as possible and with a high degree of reliability and quality of supply. One of these standards that must be met is the MG power quality (PQ). Harmonics distortion and voltage stabilization are listed as major PQ issues in the literature which may result from loads nonlinearity due to the presence of electronic devices and drives in consumers' premises, and sources uncertainty due to both of generation intermittency of renewable sources and the electronic interface devices.

Passive, active and hybrid power filters can be used for mitigating harmonic distortion. In [2] two-stage filtering station of a PV power plant to eliminate the output harmonics from the PV inverters, and improve the power quality at PCC was studied. Moreover, the transformer integrated filtering system (TIFS) was used for PQ enhancement throughout its ability of harmonic suppression [3].

Meanwhile, multifunctional voltage source inverters or flexible alternating current transmission system (FACTS) devices are utilized to process these problems that may yield voltage instability in the MG. The unified power flow conditioner (UPFC) on the transmission level provides the controlling of power flow [4]. For distribution systems, the dynamic voltage restorer (DVR) is employed to compensate voltage sag [5], [6], and the distribution synchronous static compensator (D-STATCOM) provides both voltage sag and reactive power compensation [7]. DVR and D-STATCOM are only useful for compensating a specific kind of power quality issues. So, it is essential to develop a new scheme of unified series-shunt compensator (USSC), which can alleviate a wider range of PQ issues. One of them is the multi-function device that is named as 'switched filter-compensator (SFC)'. It can be exploited for mitigating harmonics distortion and voltage stabilization as well. It acts with trial and error-tuning for a specific operating condition. As applications of the SFC, it has been used to enhance the PQ and voltage stabilization of induction motors [8]. Furthermore, hybrid SFC driven by two regulators and one of two schemes of FACTS topologies have been applied to an MG aiming to mitigate harmonics and improving both power factor and voltage stability [9]. SFC topology for wind energy in a grid-connected system is studied in [10] to prove its capability of harmonics reduction at different conditions (load variation and fault conditions) and compensating the reactive power to satisfy the dynamic voltage stability.

This paper presents a modification of the SFC to act adaptively with self-tuning as the operating conditions are subjected to change during MG operation. The proposed device is named as 'adaptive switched filter-compensator (ASFC)'. In addition, the gains of the proportional integral derivative

(PID) controller, which is an element in the ASFC topology is optimally tuned using the grasshopper's optimization algorithm (GOA) [11]. The GOA parameters are used to verify the GOA-PID controller's performance by searching for PID controller gains with an objective of minimizing the integral time absolute error (*ITAE*). This helps achieve fast processing and more accurate results rather than those obtained by trial and error method. Moreover, D-STATCOM is developed to be a self-tuning device. Comparative studies are introduced in this study including different cases to illustrate, to any extent, the effectiveness of applying either the ASFC or the developed D-STATCOM to an isolated MG. The MG comprises renewable energy sources (RESs) such as solar PV energy, wind energy system (WES), battery energy storage system (BESS) and the proton exchange membrane fuel cell (PEMFC) supplying AC loads at the point of common coupling (PCC). More details about the MG architecture and the mathematical modelling of its components, which the simulation modelling is based on, are described in the next section. The results of applying the proposed ASFC to the case studies confirm that it provides more accurate solution at less computation time. The main contributions of this work can be summarized as:

- A proposed ASFC with optimal tuned PID controller is introduced.
- A modified model of D-STATCOM with optimal tuned PID controller using GOA is presented.
- Different case studies are performed considering the features of RESs and temporary fault conditions in order to validate the effectiveness of the proposed devices.

Accordingly, this paper is organized as follows. In section II, the architecture of MG is illustrated. Section III presents a modification of the ASFC for mitigating power quality problems. In section IV, the results of applying either ASFC or D-STATCOM are examined by using different case studies. Finally, the conclusions are introduced in section V.

II. ISOLATED MG ARCHITECTURE

The MG central controller (MGCC) manages the operation of integrated DERs and loads. Each of DERs is connected to a local controller (LC) to adopt their reliable and economical operation. The main tasks of MGCC can be summarized as:

- Providing the individual power and voltage set point for each power flow/DER control strategy.
- Satisfying the electrical loads' requirements.
- Alleviating emissions and network losses.
- Exploiting the operational efficiency of the DERs.

The proposed MG includes solar PV, WES, BESS and PEMFC. Each of these resources is connected to its LC, which in turn is connected to the MGCC. The MGCC can be connected to the host (or utility) grid through the distribution system operator (DSO) if it is desired or needed. The LC encompasses a breaker for switching operation of its connected resource and maximum power point tracking (MPPT) circuit. DER-bus is connected to the load-bus at 380V, 50 Hz.

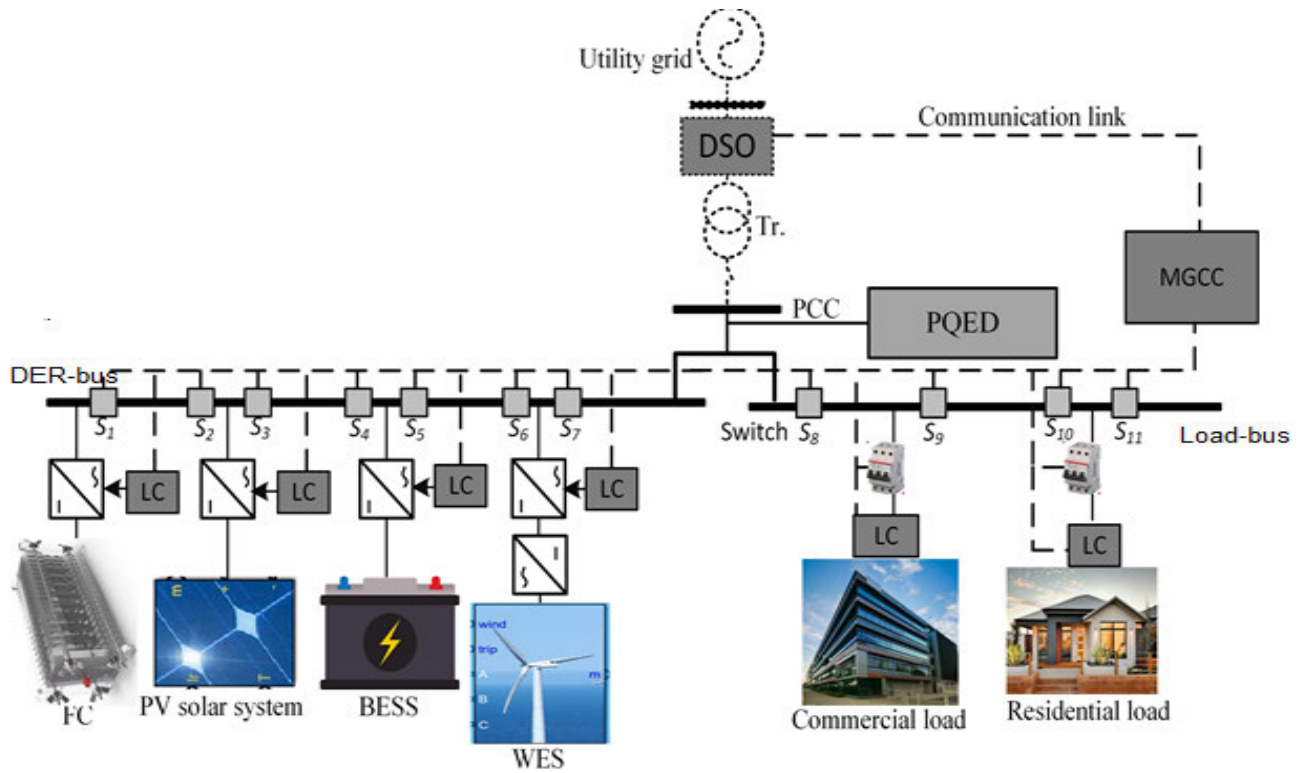


FIGURE 1. Diagram of an isolated MG with control system structure including ASFC.

Fig. 1 shows the isolated MG with a control system structure including the power quality enhancement device (PQED) at the PCC.

A. MATHEMATICAL MODEL OF THE SOLAR PV

The PV generation power output, P_{PV} , can be calculated as:

$$P_{pv} = \eta_g N_{pv} A_m G_t \quad (1)$$

where:

η_g : The instantaneous efficiency of the PV generator.

N_{PV} : The number of modules.

A_m : The area of one module used in a system (m^2).

G_t : The global irradiance incident on the titled plane (W/m^2)

The efficiency of the PV generator instantly is denoted as:

$$\eta_g = \eta_r \eta_{pt} [1 - \beta_t(T_c - T_r)] \quad (2)$$

where η_r is the PV reference efficiency of the generator, η_{pt} is the power tracking equipment efficiency, which equals 1 when using a perfect maximum power point tracker. T_c and T_r are the PV cell and reference temperatures in $^{\circ}C$, respectively. β_t is the efficiency temperature coefficient [12].

The artificial neural network (ANN) is used to forecast the required voltage value at the MPP [13] at which the desired duty cycle of the boost converter is calculated. The ANN comprises of three layers; (i) the input layer that has two neurons corresponding to the irradiation and temperature, (ii) the hidden layer including 10 neurons, and (iii) the output

layer with one neuron. The maximum number of epochs to train the ANN equals 100 and the learning rate equals 0.02. The parameters of the PV model are specified from a practical PV module (KC200GT) manufactured by KYOCERA [14] as given in Table 11, (Appendix A). The LC of the PV system is designed for extracting the power when: $0 \leq T_c \leq 60$ & $100 \leq G_t \leq 1000$.

B. MATHEMATICAL MODEL OF THE WES

The wind turbine generator power output can be determined as:

$$P_w = \begin{cases} 0, & V < V_{ci} \\ aV^3 - bP_r, & V_{ci} \leq V < V_r \\ P_r, & V_r \leq V < V_{co} \\ 0, & V \geq V_{co} \end{cases} \quad (3)$$

where $a = \frac{P_r}{(V_r^3 - V_{ci}^3)}$, $b = \frac{V_{ci}^3}{V_r^3 - V_{ci}^3}$, P_r is the rated power of the wind generator. V_{ci} , V_{co} , and V_r are the cut-in, cut-out and rated speeds of the wind turbine [15]. The extracted real power from the wind turbine is denoted by:

$$P_w = \frac{1}{2} \rho A C_p(\lambda, \beta) \left[\frac{R \omega_{opt}}{\lambda_{opt}} \right]^3 \quad (4)$$

where ρ is the density of the air ($\rho = 1.2250 \text{ kg/m}^3$), A is the blade swept area, R is the length of the blade, ω_{opt} is the optimum speed of wind turbine and λ_{opt} is the optimum tip-speed ratio. The power coefficient C_p is a function of the pitch

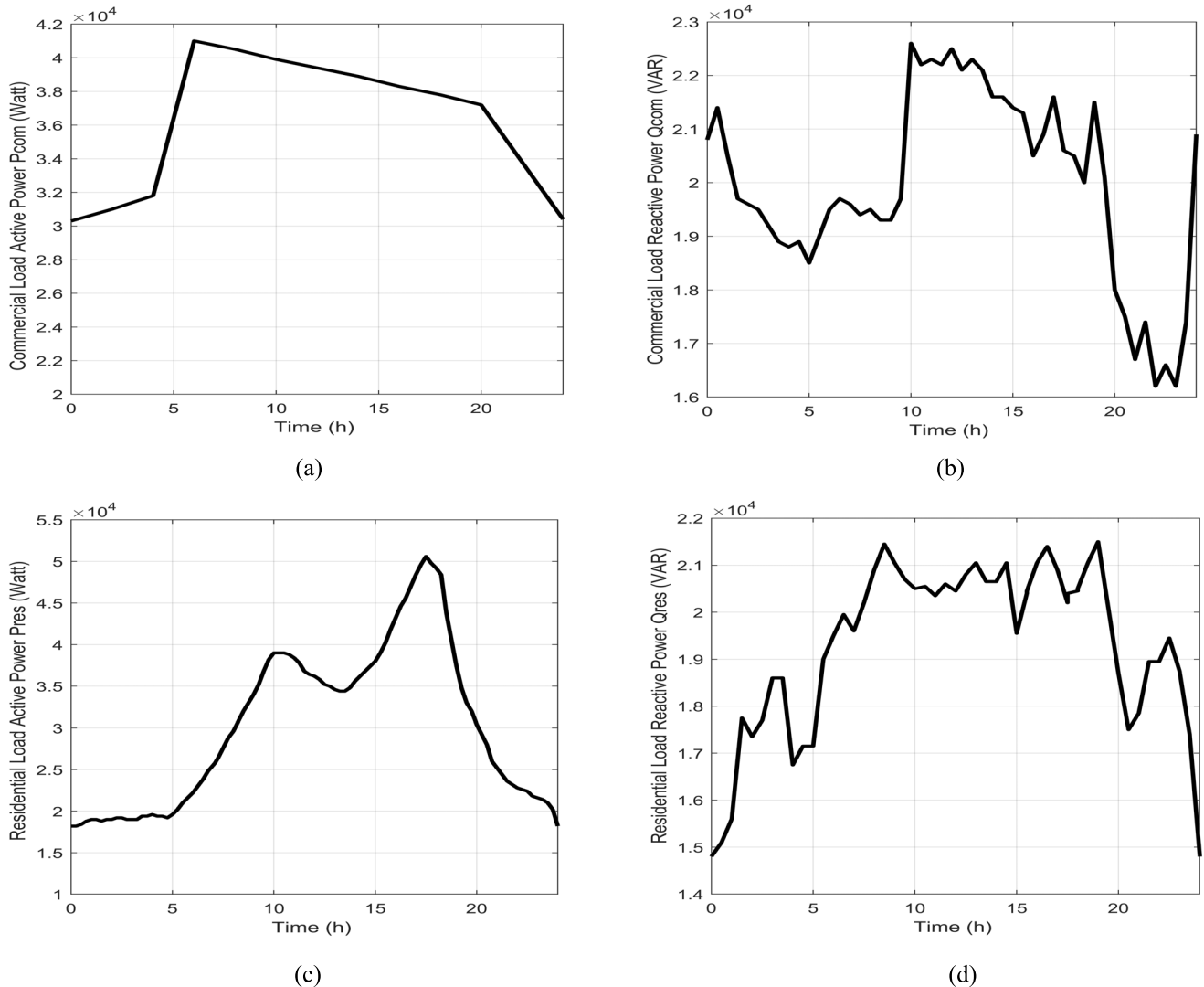


FIGURE 2. The load profile curves of (a) commercial load active power (P_{com}), (b) commercial load reactive power (Q_{com}), (c) residential load active power (P_{res}), (d) residential load reactive power (Q_{res}).

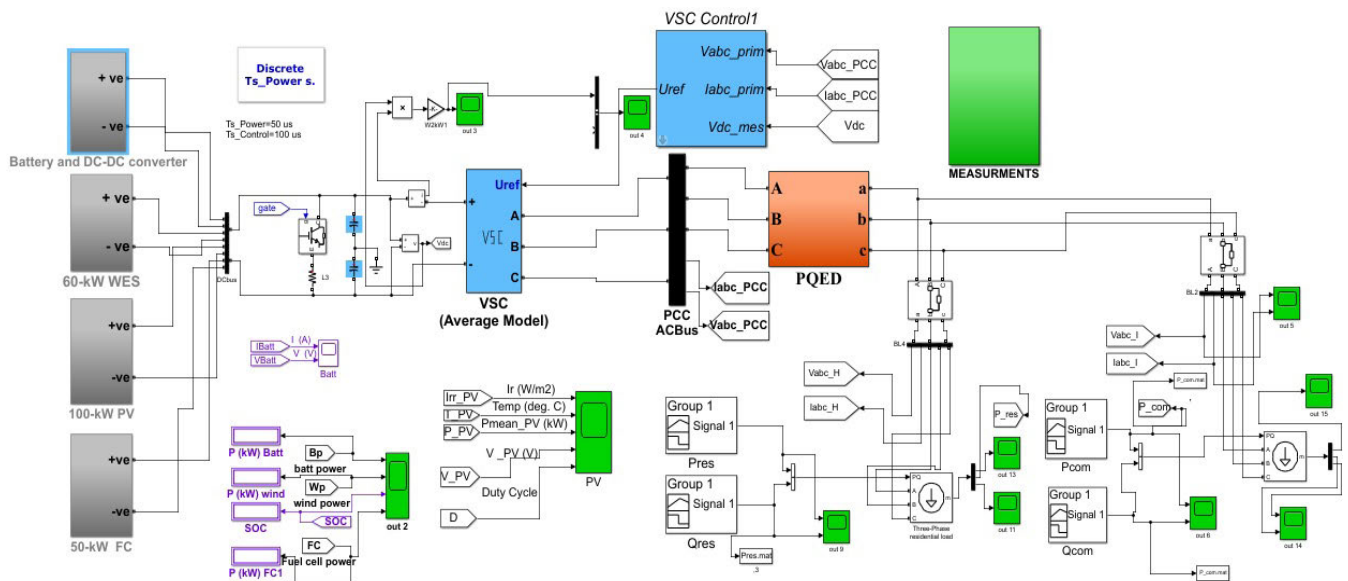


FIGURE 3. The MATLAB/SIMULINK modeling of the proposed MG.

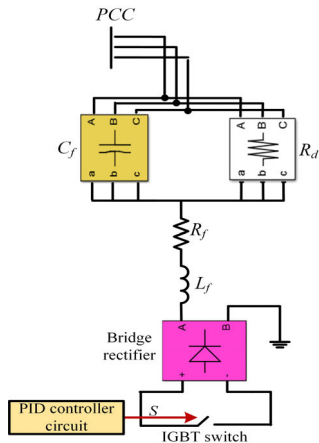


FIGURE 4. The proposed ASFC.

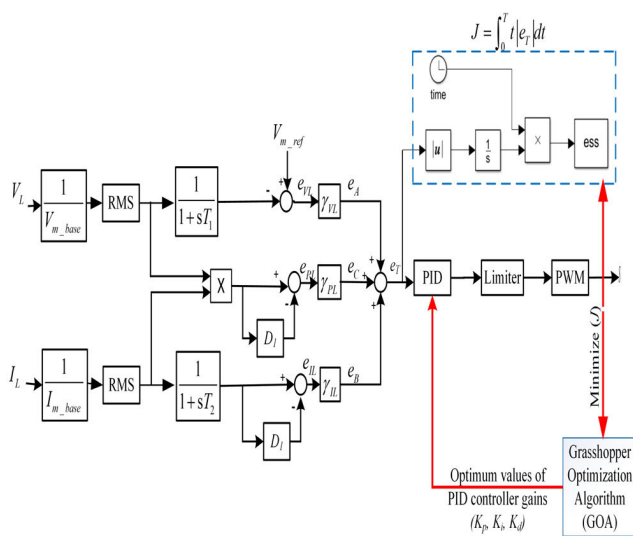


FIGURE 5. The PID controller using (GOA) with PWM circuit.

angle β and the tip speed ratio λ , which is given by:

$$\lambda = \frac{\omega R}{V_w} \quad (5)$$

where ω is the rotational speed of the wind turbine and V_w is the wind speed. The MPPT is carried out by using the perturbation and observation (P&O) technique [16]. The parameters of the WES model are specified from practical data (E3120) manufactured by ENDURANCE [17] as given in Table 12 (Appendix A).

C. BESS MODELLING

The battery bank is used for storing/supplying electrical energy in case of charging/discharging process. The most frequent type used is the lead-acid. The accessible battery bank capability at hour t during charging/discharging can be expressed as:

$$C_{bat} = C_{bat}(t - 1)(1 - \sigma) \pm \left[\frac{E_{load}(t)}{\eta_{inv}} - E_{pv(t)}E_w(t) \right] \eta_{bat} \quad (6)$$

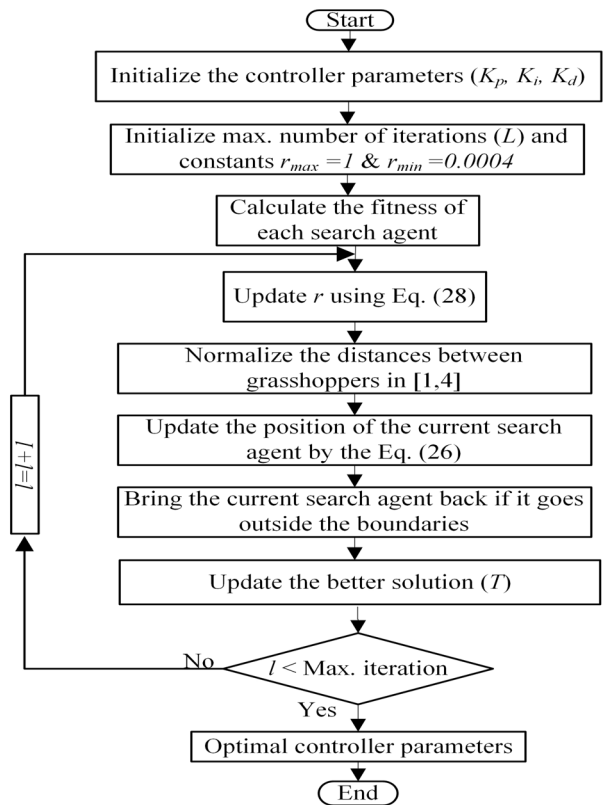


FIGURE 6. The implementation of the GOA technique for determining the controller parameters.

where $C_{bat}(t)$ and $C_{bat}(t - 1)$ are the battery bank capacity in (Wh) at the hour (t) and ($t - 1$), respectively. η_{bat} is the efficiency of the battery, σ is the self-discharge rate of the battery bank. $E_{pv}(t)$ and $E_w(t)$ are the PV and wind-generated energies, respectively. $E_{load}(t)$ is the load energy consumption of the MG at hour (t) and η_{inv} is the inverter efficiency [18].

The positive and negative signs refer to the charging and discharging state, respectively. The aim of the battery LC is to control the charging and discharging of the battery according to the renewable power, state of charge (SoC) and load demand available. The battery's SoC is provided by:

$$SoC = SoC_0 - \frac{1}{C_{nom}} \int_{t_0}^t I_{bat}(t)dt \quad (7)$$

where C_{nom} and $I_{bat}(t)$ are the battery capacity (Ah) and the battery current (A), respectively [19]. The parameters of the BESS model are specified from real BESS data (S2-2160GEL) manufactured by Rolls battery [20] as given in Table 13 (Appendix A).

D. PEMFC MODELLING

The PEMFC is the most common type of FCs and the best choice for housing and vehicle applications because of its

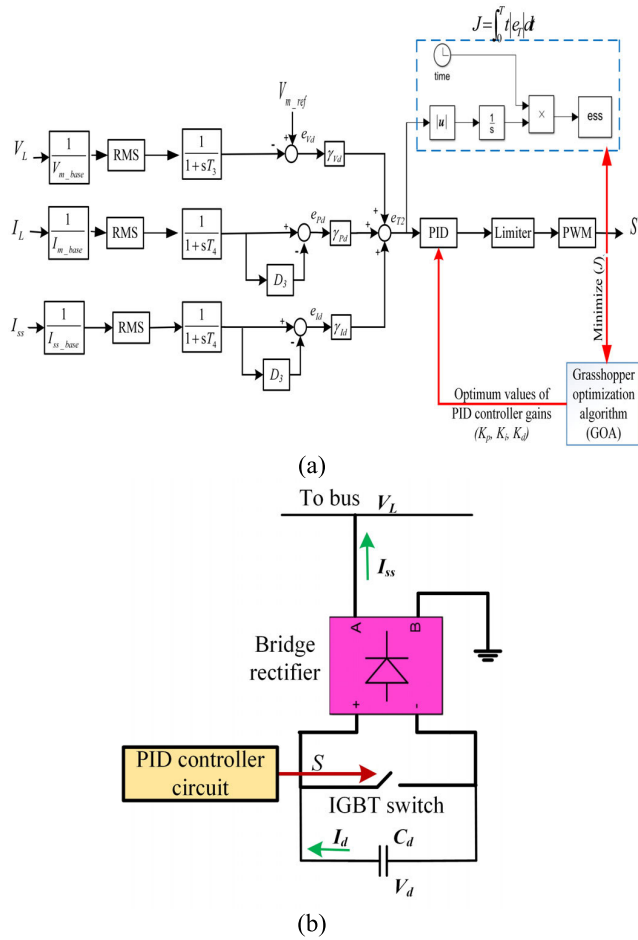


FIGURE 7. The Controller scheme of modified D-STATCOM, (a) the block diagram of D-STATCOM, and (b) D-STATCOM configuration with three-level error-driven PID.

performance features such as fast start-up, lightweight and high-power density.

The FC parameters, in general, such as open-circuit voltage (E_{oc}), the exchange current (I_c) and the Tafel slope (A) depends on variations in temperature, pressures, compositions and flow rates of fuel and air. Therefore, to calculate the FC parameters, the following formulas are used:

$$V_{fc} = \left(E_{oc} - NA \ln\left(\frac{I_{fc}}{I_c}\right) \times \frac{1}{s\frac{T_d}{3} + 1} \right) - RI_{fc} \quad (8)$$

and

$$E_{oc} = K_c E_n \quad (9)$$

$$I_c = \left(\frac{zFk(P_{H2} + P_{O2})}{Rh} \right) e^{\left(\frac{-\Delta G}{RT}\right)} \quad (10)$$

$$A = \frac{RT}{z\alpha F} \quad (11)$$

where K_c is the voltage constant in nominal operating condition (V), E_n is Nernst voltage, which is the thermodynamic voltage of the cells and relies on the temperature and partial pressure of reactants and products inside the stack (V), R is universal gas constant (8.31450 J/(mol. K)), F is Faraday's

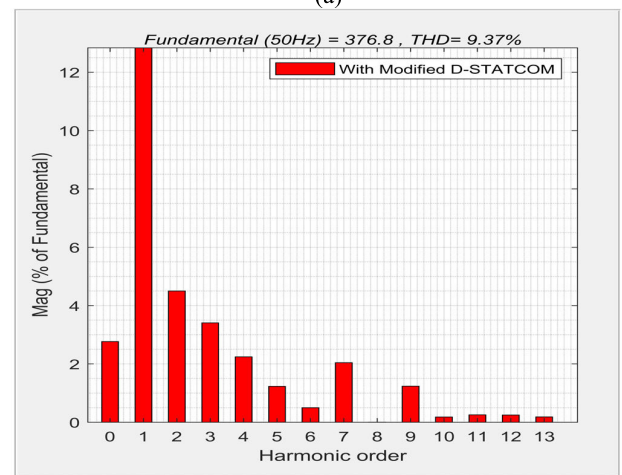
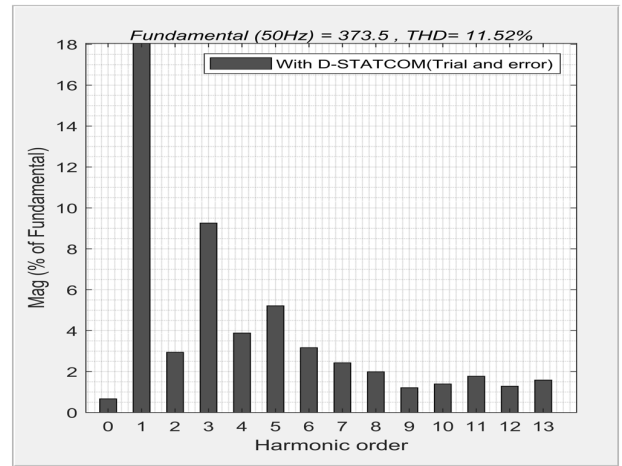


FIGURE 8. The THD_V of the voltage at the PCC (a) with the traditional D-STATCOM, (b) with the modified D-STATCOM.

constant (964850 A.s/mol), z is number of electrons moving, α is charge transfer coefficient, T is the operating temperature (K), P_{H2} and P_{O2} are partial hydrogen and oxygen pressures inside the stack (atm), respectively, k is the constant of Boltzmann (1.380×10^{-23} J/K), h is the constant of Planck (6.6260×10^{-34} J.s), and ΔG is the size of the activation barrier which depends on the type of electrode and catalyst used [21].

Table 14. shows the parameters of the PEMFC model, which are specified from real data (PowerCells S3) manufactured by POWERCELL [22]. The LC of the PEMFC is designed for extracting power at $P_{H2} \geq 4$ bar.

E. THE LOAD LOCAL CONTROLLER (LLC)

Real load data is given from Hurghada city, Egypt. It consists of two daily load curves for active and reactive power of (i) commercial load as shown in Fig. 2a,b, and (ii) residential load as shown in Fig. 2c,d.

Based on the mathematical models of each component of the MG, the overall structure of the MG simulation model including a PQED is shown in Fig. 3. It is to be noted that

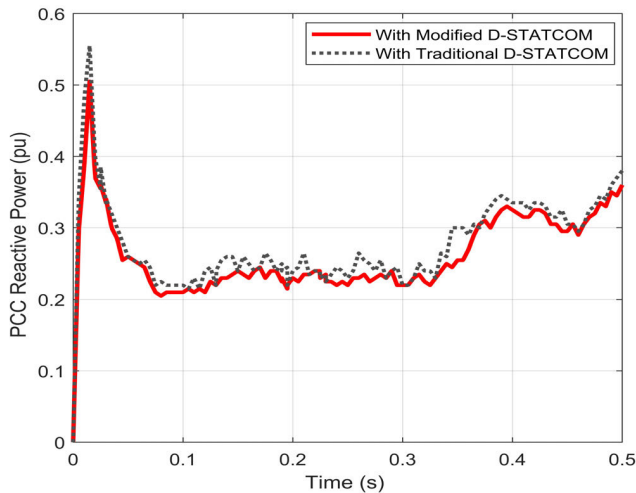


FIGURE 9. The reactive power at the PCC with traditional and modified D-STATCOM.

TABLE 1. PID controllers’ gains for modified and traditional D-STATCOM.

Control parameters	Modified D-STATCOM	Traditional D-STATCOM
K_p	22.523	12.5
K_i	17.125	26.7
K_d	8.642	14.3

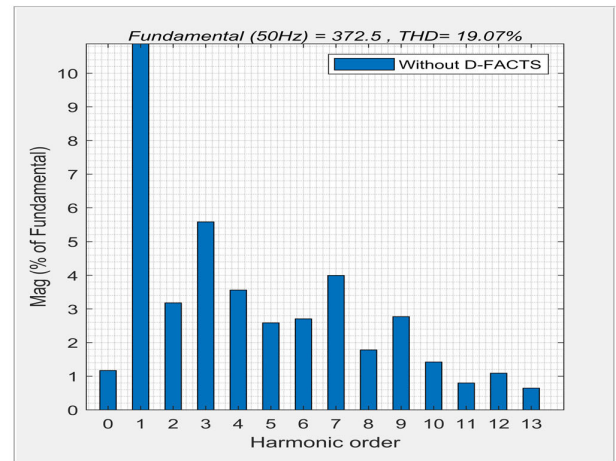
the simulation model leads to results that may differ from the practical solutions because of the delays occurred in real system (in measuring paths, data processing and execution systems).

III. ADAPTIVE SWITCHED FILTER COMPENSATOR (ASFC)

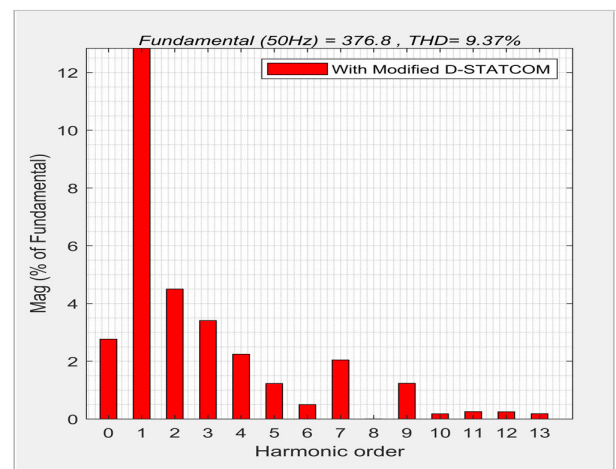
To improve the performance of the isolated MG, the proposed ASFC is applied to the load bus at PCC. The ASFC is a switched/modulated filter that consists of a fixed shunt condenser bank linked to the AC side of an uncontrolled rectifier’s arm. The proposed ASFC is a low-cost device compared to other shunt-connected FACTS devices, e.g., the D-STATCOM as reported in Reference 7. It only uses one solid-state low-power switch with a 2-pulse low rating diode rectifier. This is approximately one-fourth of the D-STATCOM cost. The ASFC construction and the PID controller circuit are shown in Figs. 4 and 5.

The proposed PID control strategy comprises of three loops as voltage stabilization loop error, current loop limiting error, and dynamic power loop error. The first loop controller input is the voltage at PCC (V_L). The aim of this loop is to reduce voltage deviations at the PCC bus voltage from a reference voltage level, i.e., a unity voltage level (V_{m_ref}). Therefore, the output is the first signal error (e_A) of the PWM, as indicated in (12) and (13), respectively.

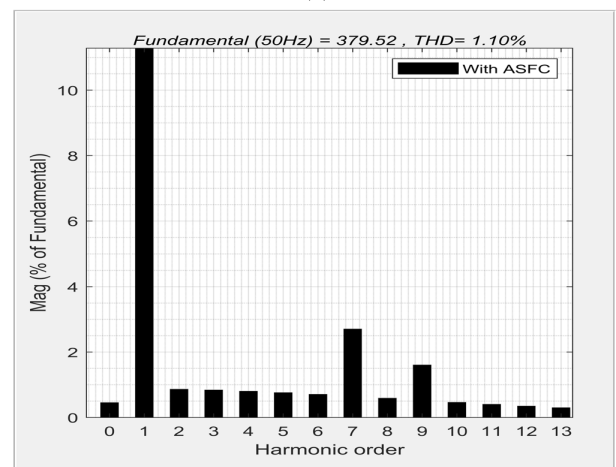
$$e_A = \gamma_{VL} \times e_{VL} \tag{12}$$



(a)



(b)

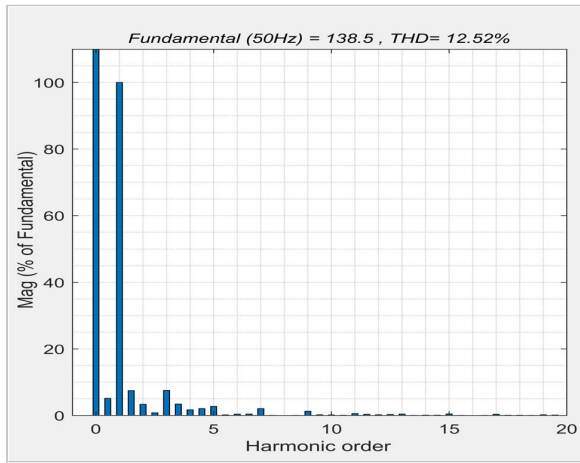


(c)

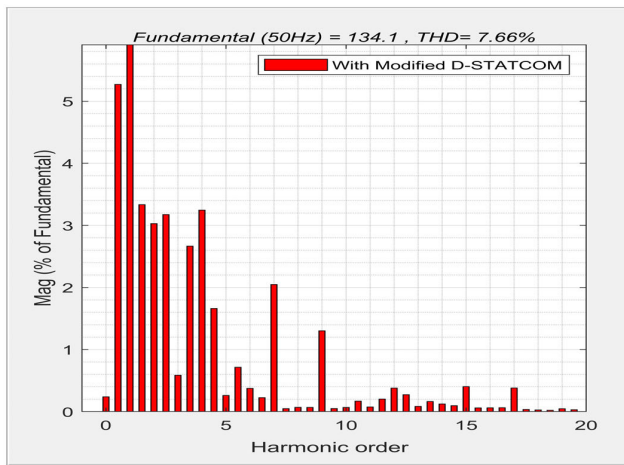
FIGURE 10. The THD_v at the PCC (a) without FACTS. (b) with modified D-STATCOM (c) with the proposed ASFC.

where:

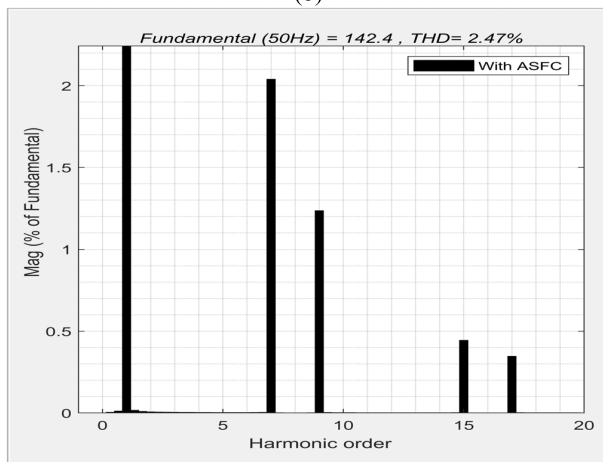
$$e_{VL} = \frac{V_{m_ref} - V_L \left(\frac{1}{1+sT_1} \right)}{V_{m_base}} \tag{13}$$



(a)



(b)



(c)

FIGURE 11. The THD_i at the PCC (a) without FACTS. (b) with modified D-STATCOM (c) with the proposed ASFC.

The input of the second loop controller is the measured current at PCC (I_L). The concept behind this controller loop is to limit the inrush current and the dynamic RMS current changes. So, the loop controller compares the current at PCC

TABLE 2. PID controllers' gains for ASFC, modified D-STATCOM for Harmonic analysis.

Control parameters	ASFC	Modified D-STATCOM
K_p	96.454	72.244
K_i	23.183	9.325
K_d	7.586	2.452

TABLE 3. PID controllers' gains for ASFC and modified D-STATCOM during PV irradiation variation.

Control parameters	ASFC	Modified D-STATCOM
K_p	40.854	85.531
K_i	32.172	25.062
K_d	12.623	4.837

with a reference value (I_{m_base}). The output of this comparison is the second signal error (e_B) as given in (14) and (15).

$$e_B = \gamma_{IL} \times e_{IL} \tag{14}$$

and

$$e_{IL} = \frac{I_L}{I_{m_base}} \left(\frac{1}{1 + sT_1} \right) \left(1 - \frac{1}{1 + sT_2} \right) \tag{15}$$

The third loop controller's inputs are the measured current and voltage at the PCC bus. This loop decreases the effects of load changes and sudden excursions of the dynamic power changes. The loop controller, therefore, compares the measured voltage V_L , current I_L , and calculates power P_L ($V_L * I_L$) with their reference values, and then feeds the third error e_C given by (16) to the PWM module.

$$e_C = \gamma_{PL} \times e_{PL} \tag{16}$$

where:

$$e_{PL} = \left(\frac{V_L}{V_{m_base}} \times \frac{I_L}{I_{m_base}} \right) \left(1 - \frac{1}{1 + sT_2} \right) \tag{17}$$

Subsequently, the total error (e_T) is calculated in terms of the three control system errors, Thus,

$$e_T(t) = e_A + e_B + e_C \tag{18}$$

The difference between the signals is processed by a PID controller to obtain the phase angles (delta) needed to drive the error to zero.

A. FORMULATION OF THE OPTIMIZATION PROBLEM

1) FITNESS FUNCTION

The fitness function, given by (19) is used to fine-tune the proposed ASFC-PID controllers' gains (K_p , K_i , and K_d).

$$\min(J) = \min(ITAE) \tag{19}$$

where J is the total controller error of the ASFC and $ITAE$. The performance index of the $ITAE$ is expressed in a mathematical term as:

$$J = ITAE = \int_0^T t |e_T| dt \tag{20}$$

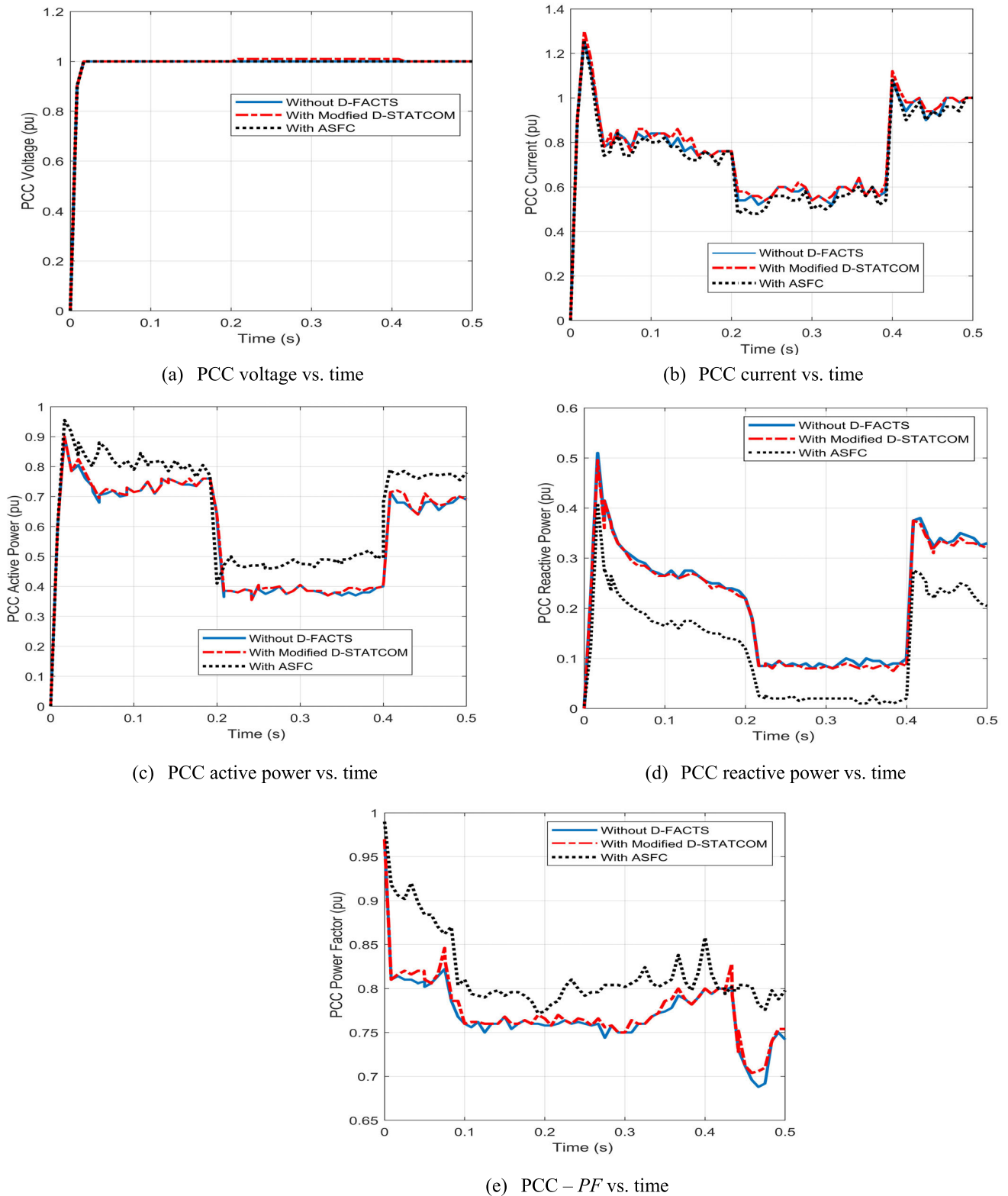


FIGURE 12. The PQ indices at the PCC using ASFC, modified D-STATCOM and without using FACTS schemes under PV irradiation variation.

2) CONSTRAINTS

- The PCC voltage level is within its limits, that is

$$0.95 \leq V_L \leq 1.05 \quad (21)$$

- Total harmonic distortion of the voltage at the PCC (THD_v), given by (22) must be following the IEEE Standard 519 [23], that is limited by a maximum value ($THD_{v,max} = 8\%$), as given in Table 15. Thus,

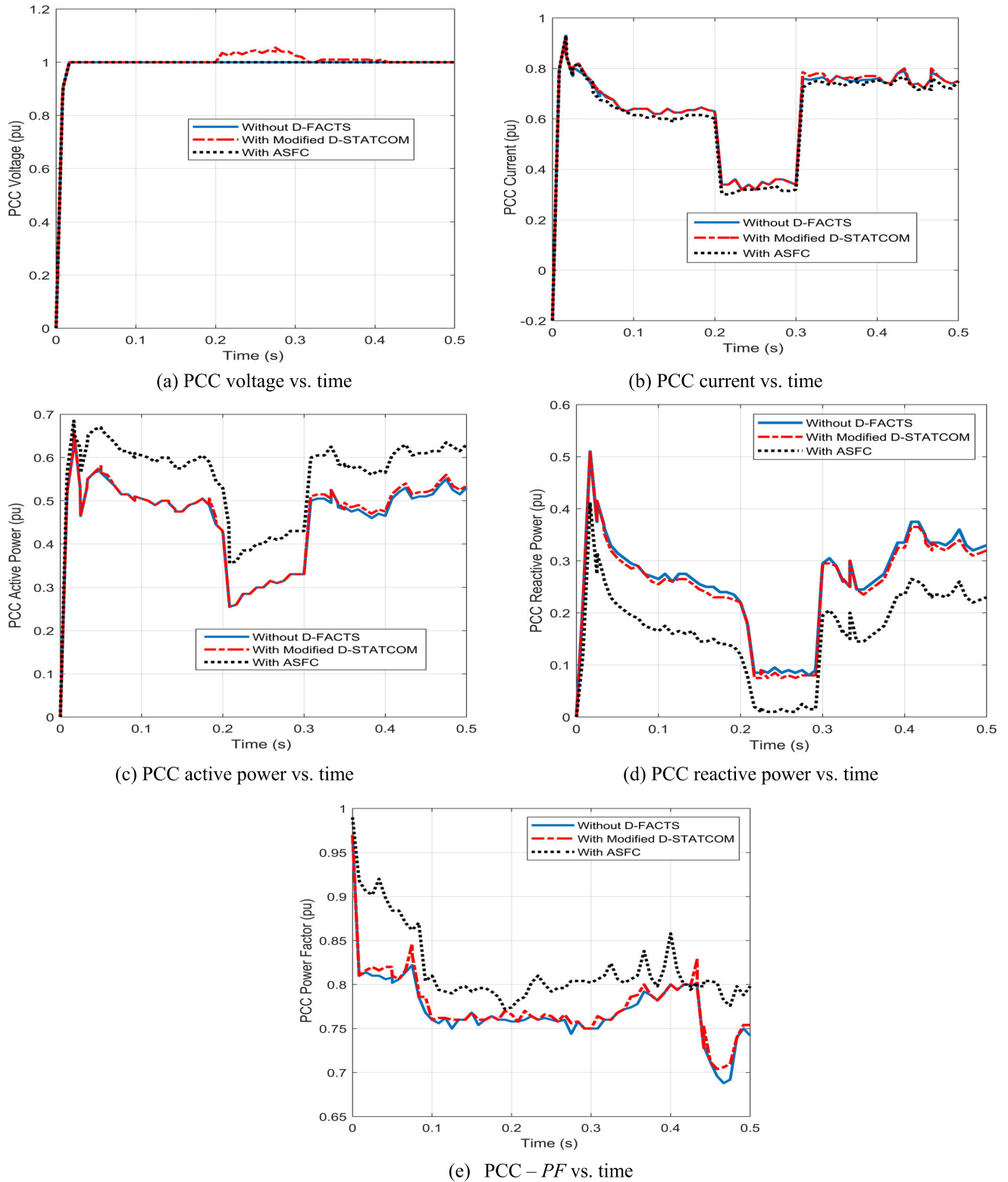


FIGURE 13. The PQ indices at the PCC using the ASFC, modified D-STATCOM and without using FACTS schemes under wind speed variation.

$$THD_v = \frac{\sqrt{\sum_{h=2}^n V_h^2}}{V_1} \quad (22)$$

$$THD_v \leq THD_{v,max} \quad (23)$$

- Total harmonic distortion of the current at the PCC (THD_i), given by (24), according to the IEEE Standard 519 [23], should be limited by a maximum value ($THD_{i,max} = 5\%$), as given in Table 16. Hence,

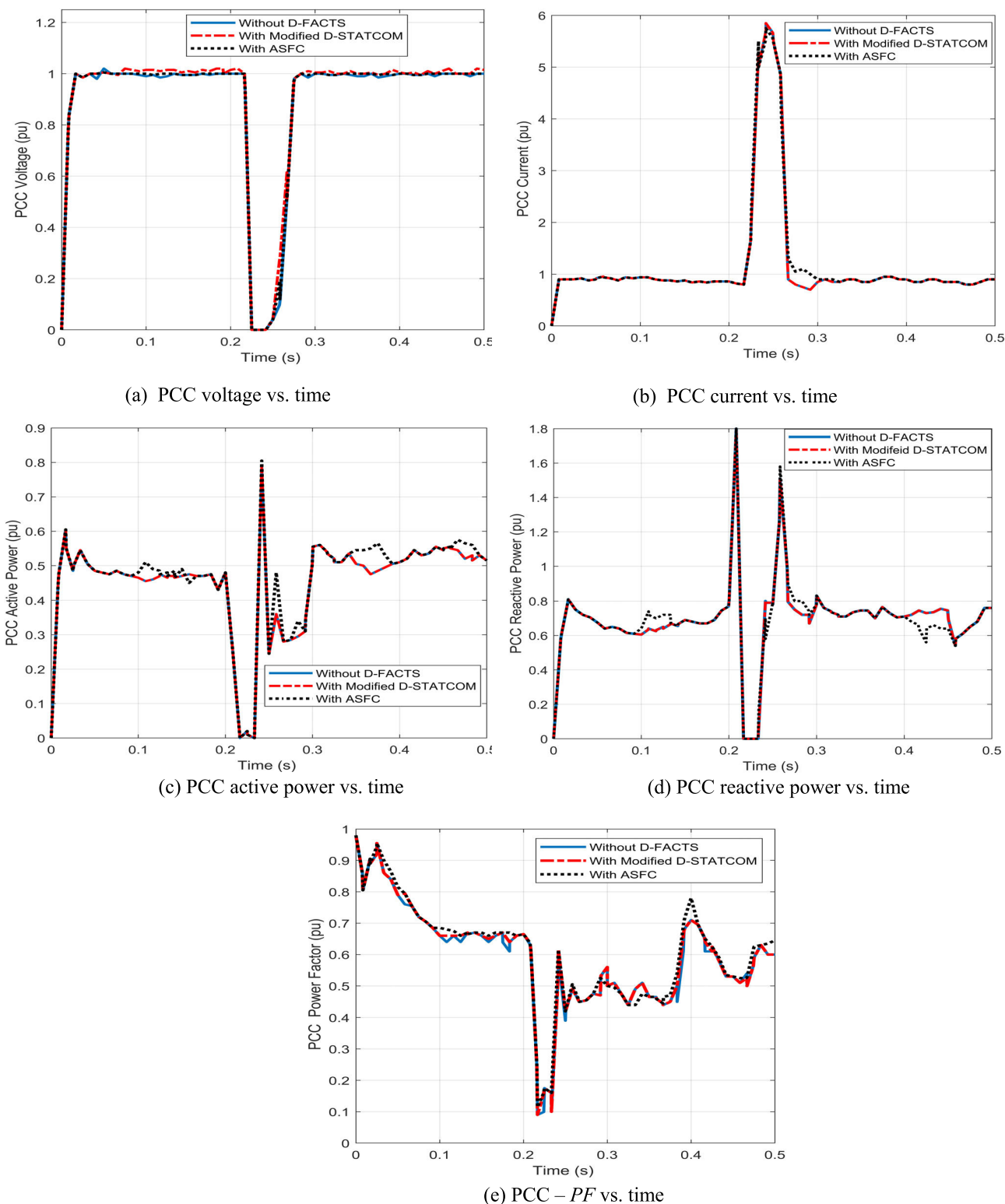


FIGURE 14. The PQ indices at the PCC using the ASFC, modified D-STATCOM and without using FACTS schemes under short circuit tests.

$$THD_i = \frac{\sqrt{\sum_{h=2}^n I_h^2}}{I_1} \tag{24}$$

$$THD_i \leq THD_{i,max} \tag{25}$$

3) IMPLEMENTATION OF THE GOA

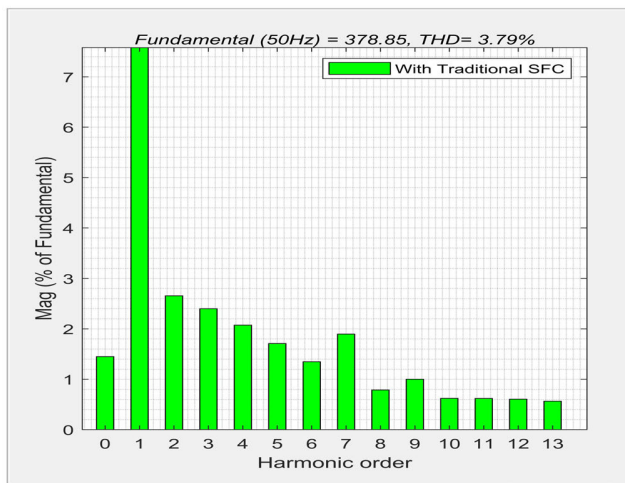
The GOA is a proposed single objective, population-based heuristic algorithm imitating grasshopper swarm’s behavior in nature and mathematically modelling it to solve

TABLE 4. PID controllers' gains for ASFC and modified D-STATCOM during wind speed variation.

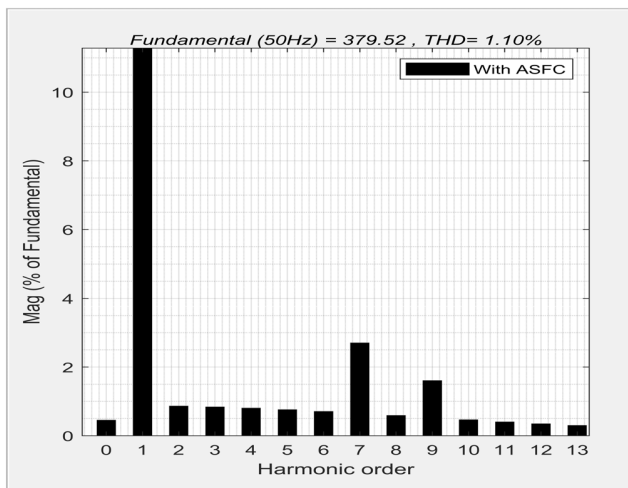
Control parameters	ASFC	Modified D-STATCOM
K_p	66.234	75.327
K_i	12.456	42.251
K_d	3.256	15.236

TABLE 5. PID controllers' gains for ASFC and modified D-STATCOM during the three-phase short circuit test.

Control parameters	ASFC	Modified D-STATCOM
K_p	90.334	75.368
K_i	82.725	38.262
K_d	29.639	12.293



(a)



(b)

FIGURE 15. The THD_v at the PCC (a) with the traditional SFC, (b) with the ASFC.

optimization problems with contentious variables [24], [25]. The algorithm simulates grasshoppers' forces of repulsion and attraction. While repulsive forces allow grasshoppers to explore the search space, they are urged by attraction forces to exploit the promising areas. GOA has been fitted with

a coefficient that reduces the distance of the grasshoppers' comfort zone to balance exploration and exploitation phases during optimization. This helps GOA not to become trapped in local optimum and find an accurate global optimum estimate. As the best solution obtained so far by the swarm considered as a target to be pursued, grasshoppers have a great opportunity to find the global optimum by improving the target through iterations. The updating position of GOA equation is obtained as

$$X_i^d = r \left(\sum_{\substack{j=1 \\ j \neq i}}^N r \frac{U_{bd} - L_{bd}}{2} S \left(\left| X_j^d - X_i^d \right| \frac{X_j - X_i}{d_{ij}} \right) \right) + T_d \tag{26}$$

where X_i^d is the position of the current solution in the d -th dimension, r is a coefficient of diminishing that narrows the zones of comfort, repulsion, and attraction. U_{bd} and L_{bd} are the upper & lower bounds in d -th dimension, d_{ij} is the distance between j -th grasshopper (X_j) and i -th grasshopper (X_i) in absolute value, S is a function that defines the social forces between grasshoppers and T_d is the target value in d -th dimension, which is the best solution found so far.

Equation (26) indicates that the grasshopper's next position relies on its current position, the position of all other grasshoppers, and the target position. The social forces function in (26) can be depicted as follows:

$$S = f e^{-\frac{l}{r}} - e^{-d} \tag{27}$$

where f is the attraction strength and l is the scale of the attractive length. To balance exploration and exploitation, the parameter r in (26) must be decreased in proportion to the number of iterations. This promotes exploitation as the number of iterations rises. This parameter also decreases the number of iterations in the comfort zone and then, it is determined as:

$$r = r_{max} - t \frac{r_{max} - r_{min}}{T} \tag{28}$$

where r_{max} & r_{min} are the maximum and minimum values that are taken as 1 and 0.0004, respectively, and t is the current iteration. T is the maximum number of iterations.

The GOA parameters used to check the GOA-PID controller's performance are:

The number of search agents and iterations are 25 and number of 20, respectively.

Fig. 6 illustrates the implementation of the GOA method for determining the controller parameters to identify the global minimum error.

B. THE MODIFIED D-STATCOM

D-STATCOM is one of the most popular fast-response D-FACTS topologies. It can be utilized to enhance poor PQ issues throughout various system conditions [26]. A modification of D-STATCOM through using a three-level PID driven-error is done to increase its effectiveness and being

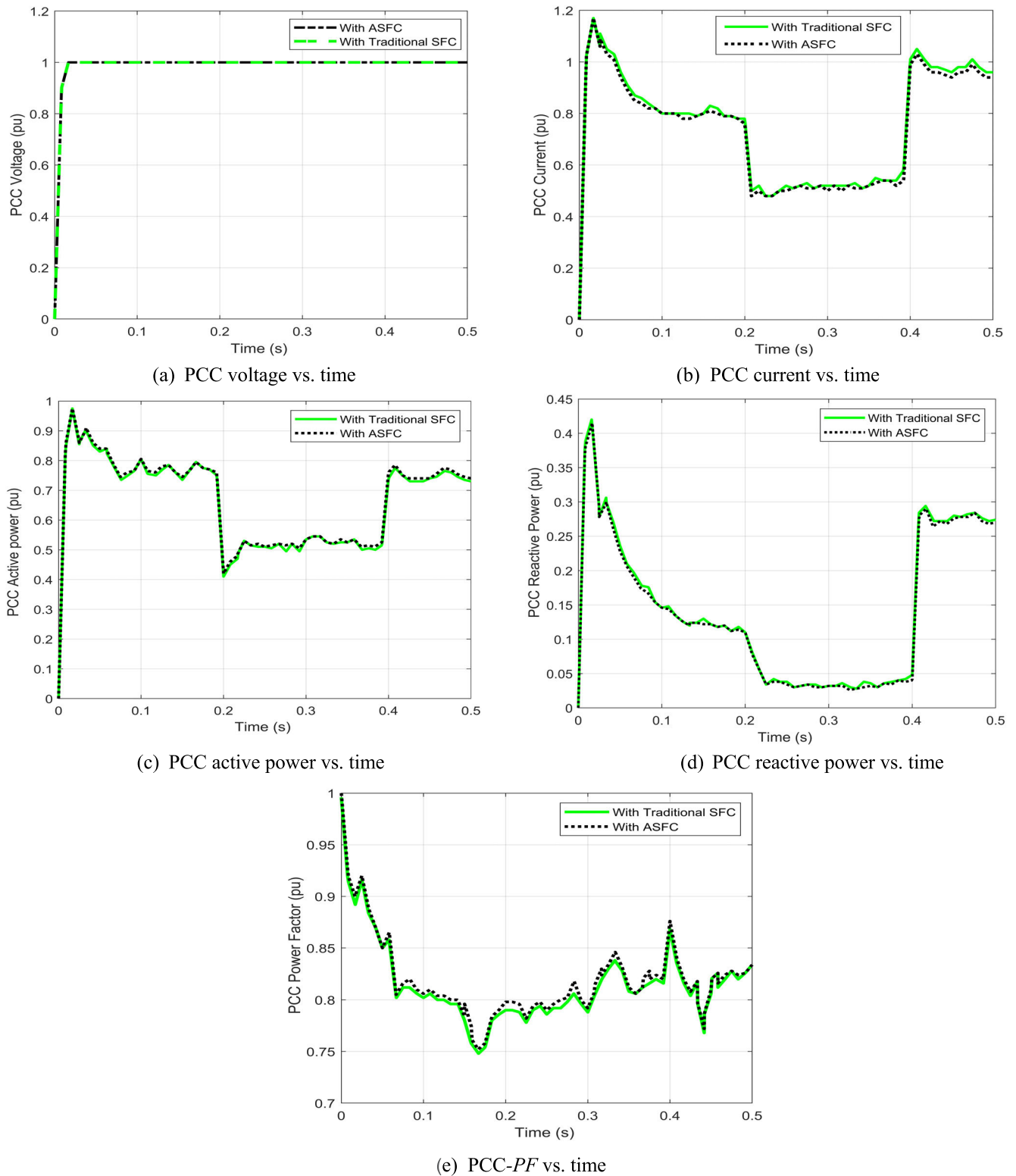
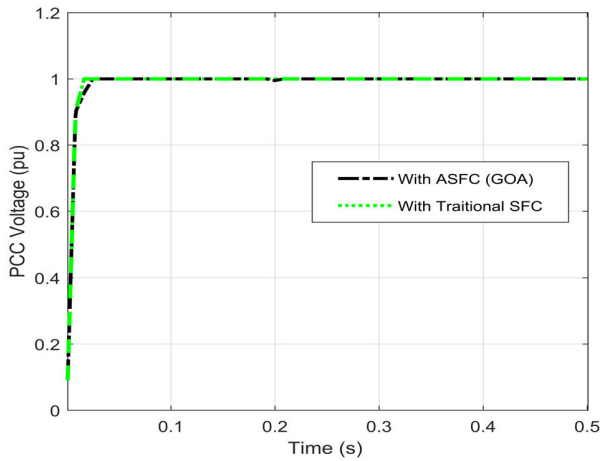


FIGURE 16. The PQ indices at the PCC using the ASFC and SFC under PV irradiation variation.

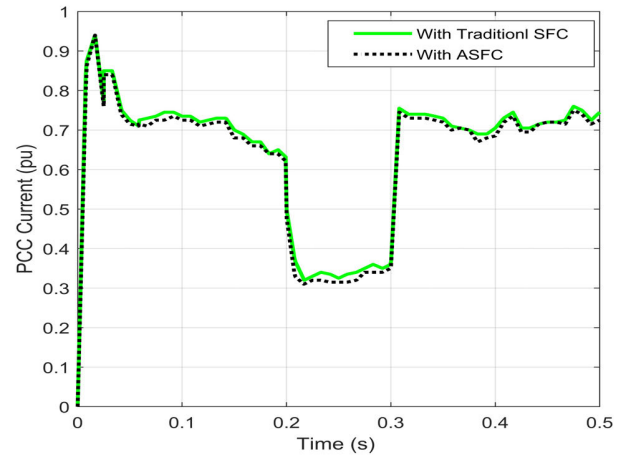
comparable to the proposed ASFC. Fig. 7 shows the controller of the modified D-STATCOM with detailed parameters given in Appendix B. The total error of D-STATCOM

can be expressed as

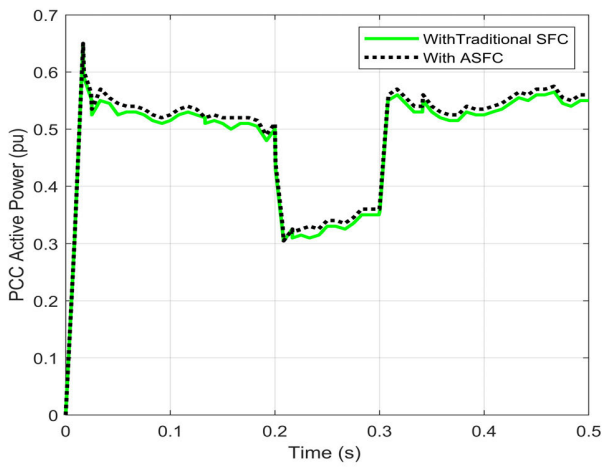
$$e_{T2} = \gamma_{vd}(e_{vd}) + \gamma_{id}(e_{id}) + \gamma_{pd}(e_{pd}) \quad (29)$$



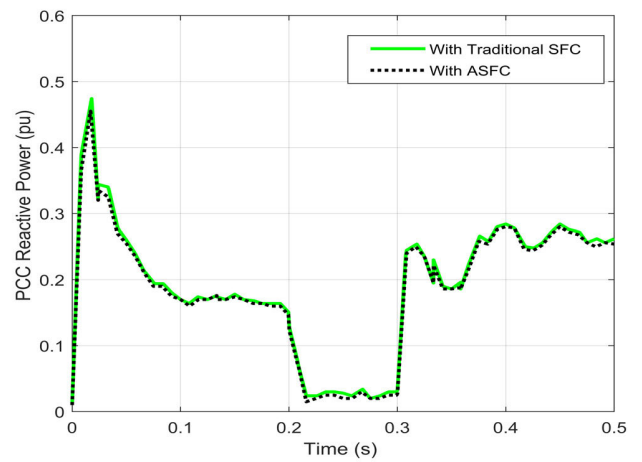
(a) PCC voltage vs. time



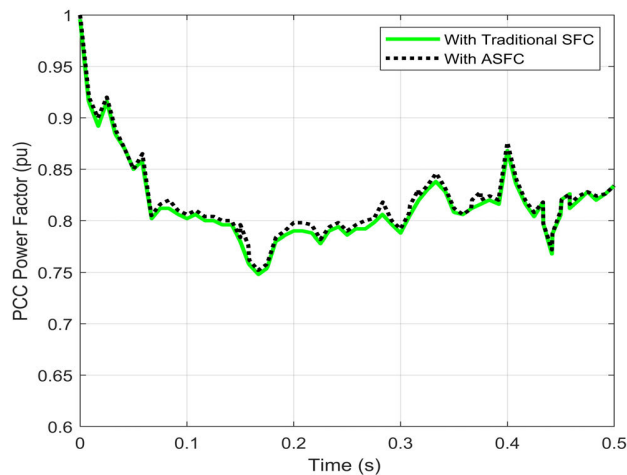
(b) PCC current vs. time



(c) PCC active power vs. time



(d) PCC reactive power vs. time



(e) PCC - PF vs. time

FIGURE 17. The PQ indices at the PCC using the ASFC and traditional SFC under wind speed variation.

IV. RESULTS AND ANALYSIS

To test the feasibility of the proposed ASFC to mitigate the harmonic distortion and improve the voltage stabilization, different case studies are discussed as in the following.

- (A) Comparison between the modified and traditional D-STATCOM.
- (B) Comparison between the ASFC and the modified D-STATCOM
- (C) Comparison between the ASFC and traditional SFC.

TABLE 6. PID controllers' gains for ASFC and traditional SFC during harmonic analysis.

Control parameters	ASFC	Traditional SFC
K_p	96.454	38.6
K_i	23.183	7.5
K_d	7.582	9.3

TABLE 7. PID controllers' gains for ASFC and traditional SFC during PV irradiation variation.

Control parameters	ASFC	Traditional SFC
K_p	30.221	25.5
K_i	11.864	21.7
K_d	42.128	52.8

TABLE 8. PID controllers' gains for ASFC and traditional SFC during wind speed variation.

Control parameters	ASFC	Traditional SFC
K_p	15.723	11.3
K_i	48.251	32.8
K_d	9.356	20.6

TABLE 9. PID controllers' gains for ASFC and traditional SFC during harmonic analysis.

Control parameters	ASFC	Traditional SFC
K_p	10.956	7
K_i	2.654	1.2
K_d	3.712	0.8

(D) Comparison with related literature.

Cases A to C are performed on the MG shown in Fig. 1 whereas case D is carried out through the system in Reference 10.

A. COMPARISON BETWEEN THE MODIFIED AND TRADITIONAL D-STATCOM

A comparison between the traditional (tuned by trial and error) and modified D-STATCOM that is tuned by the GOA for harmonic mitigation and reactive power compensation at the PCC is described. The THD_v is the main index for quantifying the level of harmonics in voltage waveforms. As shown in Fig. 8, the results obtained by using the modified D-STATCOM yield a better reduction in the THD_v as well as less reactive power received at the PCC, Fig. 9. The results satisfy the effectiveness of the modification. The controller parameters of both modified and traditional D-STATCOM are tabulated in Table 1.

B. COMPARISON BETWEEN THE ASFC AND THE MODIFIED D-STATCOM

Different scenarios such as harmonic distortion analysis, PV irradiation variation, wind speed variation and short circuit

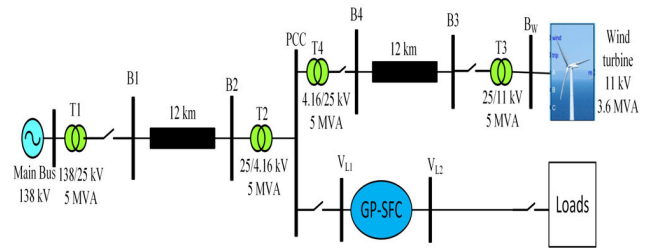
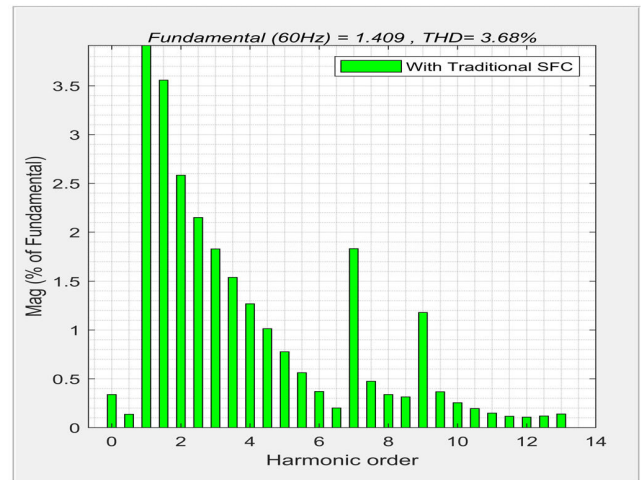
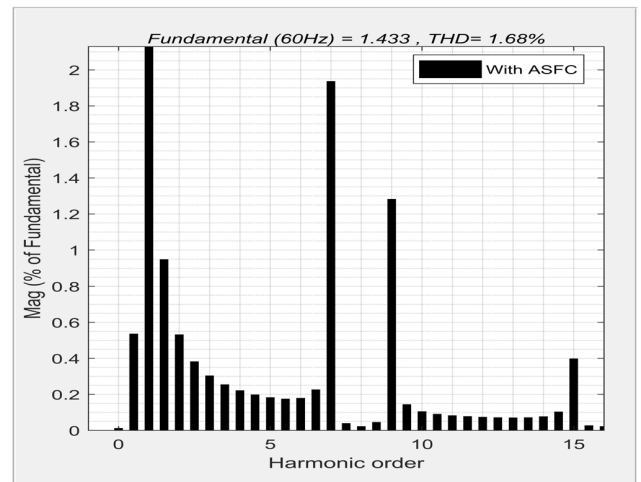


FIGURE 18. The compared system using SFC with trial and error for tuning PID controller.



(a) Frequency spectrum with SFC



(b) Frequency spectrum with ASFC

FIGURE 19. The THD_v at the PCC (a) with the traditional SFC [10], (b) with the ASFC.

test at the PCC are considered. For each scenario, the results obtained from the original system without FACTS devices are the base of comparison with those resulted when using the proposed ASFC or the modified D-STATCOM.

1) HARMONIC ANALYSIS

The THD_v and THD_i at the PCC are measured and compared as shown in Figs. 10 and 11, respectively. For the

TABLE 10. PID controllers' gains for ASFC and traditional SFC during wind speed variation.

Control parameters	ASFC	Traditional SFC
K_p	8.962	7
K_i	0.423	1.2
K_d	0.946	0.8

TABLE 11. The parameters of the PV module.

Open circuit voltage (V_{OC})	32.9V
Short circuit current (I_{SC})	8.21A
Module voltage at the maximum power point	26.3V
Module current at maximum power point (I_m)	7.61A
Maximum Power (P_m) of a PV module	200W
Reference temperature	25°C
Reference solar radiation	1000W/m ²
No. of series PV modules in a string	8
No. of parallel-connected PV strings	63

TABLE 12. The wind generations specification.

Rated Power (kW)	V_{ci} (m/s)	V_{co} (m/s)	V_r (m/s)	Hub Height (m)	Swept Area (m ²)
60	2.5	16	12	12	10.235

TABLE 13. The parameters of BESS.

Capacity (Ah)	Efficiency (%)	Min. charge (%)	Max. charge (%)	Maximum discharging rate	Max. charging rate
2160	85	20	80	20 kW	-40 kW

TABLE 14. The parameters of PEMFC.

Type	Stake Nominal power	Nernst Voltage (E_n)	Fuel cell resistance
PEM	50 kW	1.1342 V	0.66404 Ω

uncompensated system, Fig. 10a shows an increased percentage of the THD_v at the PCC. On the other side, using the modified D-STATCOM has the effect of reducing this value as shown in Fig. 10b. A more reduction of this value is noticed when using ASFC as shown in Fig. 10c. Similarly, results for the THD_i can be noticed from Fig.11. The results show the effectiveness of the proposed ASFC as the reduction of THD_i is greater than those using the modified D-STATCOM or the original system without compensation. The parameters of both ASFC and D-STATCOM controllers are given in Table 2.

2) PV IRRADIATION VARIATION

When the irradiation is suddenly reduced from 500 to 200 W/m² at $t = 0.2$ s and then increased to 500 W/m² at $t = 0.4$ s, the simulation results for the PQ indices at

TABLE 15. Voltage distortion limits.

Bus Voltage (V)at PCC	Individual harmonic (%)	Total harmonic distortion THD (%)
$V \leq 1$ kV	5.0	8.0
$1kV < V < 69kV$	3.0	5.0
$69kV < V \leq 161kV$	1.5	2.5
$161kV \leq V$	1.0	1.5

TABLE 16. Current distortion limits for systems.

MAXIMUM HARMONIC CURRENT DISTORTION IN PERCENT OF I_L					
INDIVIDUAL HARMONIC ORDER (ODD HARMONICS)					
I_{sh}/I_L	$3 \leq H < 11$	$11 \leq H < 17$	$17 \leq H < 23$	$23 \leq H < 35$	TDD
<20	4.0	2.0	1.5	0.6	5.0
20<50	7.0	3.5	2.5	1.0	8.0
50<100	10.0	4.5	4.0	1.5	12.0
100<1000	12.0	5.5	5.0	2.0	15.0
>1000	15.0	7.0	6.0	2.5	20.0

the PCC such as bus voltage (V_{rms}), current (I_{rms}), active power (P), reactive power (Q) and power factor (PF) in per unit, respectively. It is remarked that during this variation, the proposed ASFC has a positive effect on the improvement of the MG's power quality and dynamic response. The active power decreases during the recovery time with a reduced dynamic response. Moreover, the reactive power consumption is reduced and then the power factor is improved rather than those using modified D-STATCOM or without compensation. The controller parameters of the ASFC and modified D-STATCOM are given in Table 3.

3) WIND SPEED VARIATION

Wind speed variation has a significant importance when studying the MG dynamic response and power quality. So, the system is tested by rising the wind speed instantly from 6 to 12 m/s at $t = 0.2$ s and then reduced to 6 m/s at $t = 0.3$ s. Fig. 13 illustrates the simulation results of the different PQ indices such as V_{rms} , I_{rms} , P , Q and PF at the PCC under the variation of the wind speed. While the results are similar, the proposed ASFC demonstrates a significant improvement in the dynamic response compared to the results of both modified D-STATCOM and uncompensated system application. It can be noticed that in Fig.13a, the voltage rate of change at the PCC bus is increased above 1 p.u when using the D-STATCOM, whereas this value is kept constant at 1 per unit with ASFC. The controller parameters of the ASFC and modified D-STATCOM are written in Table 4.

4) SHORT CIRCUIT TEST

The MG is studied when a fault occurs at the PCC to indicate the flexibility and the dynamic response of the proposed ASFC. For instance, three-phase short circuit is applied at $t = 0.2$ s, then, cleared after 0.03 s, i.e., at $t = 0.23$ s. The V_{rms} and I_{rms} are shown in Figs. 14a,b. It is remarked that the

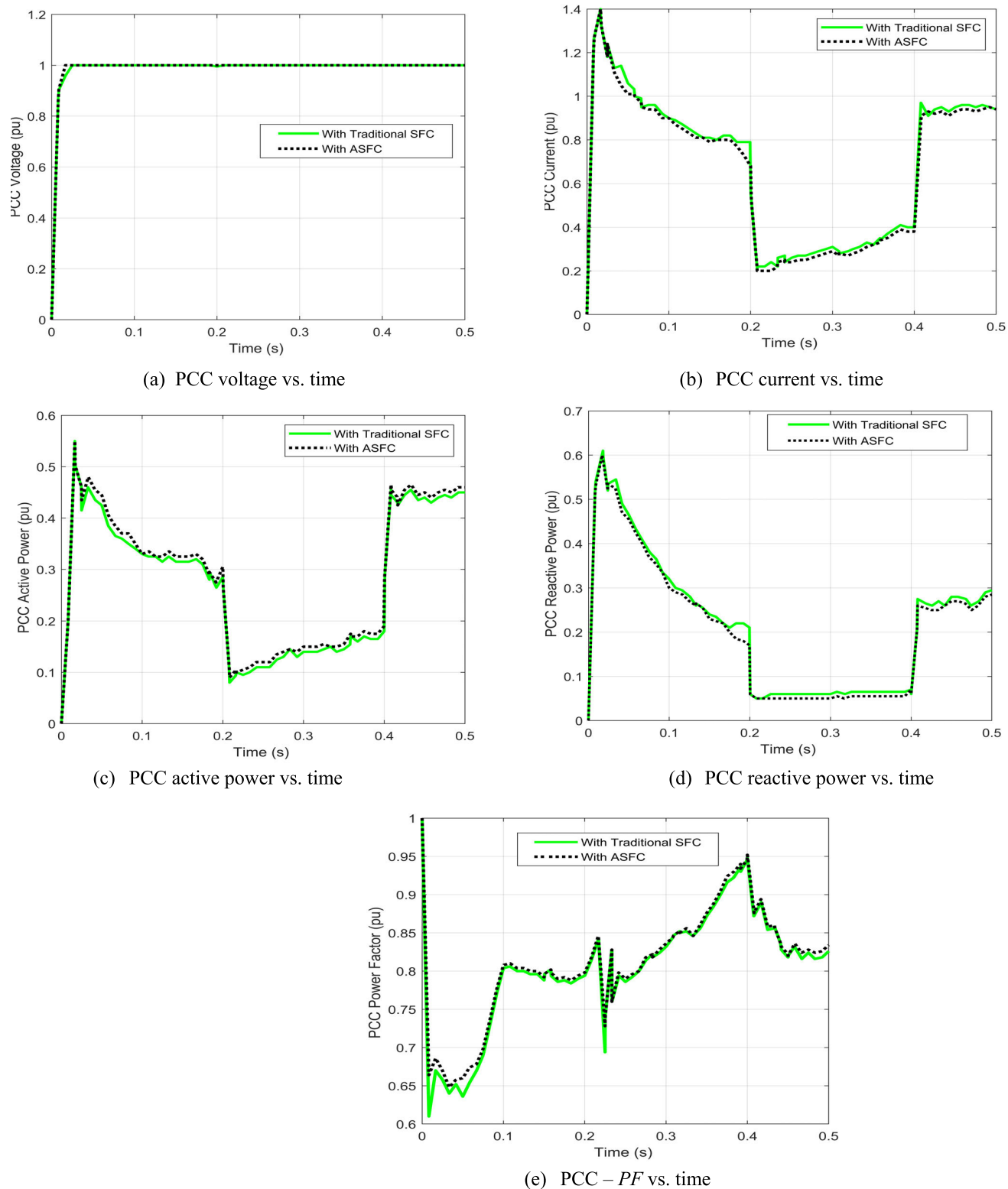


FIGURE 20. The PQ indices at the PCC using the ASFC and traditional SFC under wind speed variation.

ASFC topology yields a better dynamic response to recover its initial state after fault occurrence compared to the respective waveforms when including modified D-STATCOM

or without compensation. The controller parameters of the ASFC and modified D-STATCOM are given in Table 5.

TABLE 17. The Controller parameters of the ASFC.

System Part	Specifications
V_{m_base}	380 V
I_{m_base}	150 A
C_{sh}	300 μ F
R_f	0.150 Ω
L_f	3.0 mH
R_d	10 k Ω
V_{m_ref}	1 pu
$\gamma_v = \gamma_l$	1
γ_p	0.5
$T_1 = D_1$	10 ms
$T_2 = D_2$	20 ms
PWM frequency	3000 Hz

C. COMPARISON BETWEEN THE ASFC AND TRADITIONAL SFC

1) HARMONIC ANALYSIS

Fig. 15 shows the THD_v at the PCC when using either traditional SFC as in Reference 10 or the ASFC. The mathematical and simulation model of the traditional SFC is given in Appendix A. It is noticed that the THD_v of the ASFC reaches 1.19%, which is lesser than that of the traditional SFC, 3.79%. Moreover, the proposed technique consumes less processing time, around 87 s compared to that of the SFC, which takes around 10 m using the same computer configuration. This shows the extent of ASFC’s ability for mitigating the harmonic distortions. The controller parameters of ASFC and traditional SFC are given in Table 6.

2) PV IRRADIATION VARIATION

The same test performed in the previous section, case B, is applied to the MG, Fig. 1, using the ASFC or the traditional SFC. The results are tackled in Fig. 16 indicating that they are better in the case of using the proposed ASFC than those of the traditional SFC. Both active and reactive power consumption are decreased resulting in an improvement in the power factor. The controller parameters of both ASFC and traditional SFC are given in Table 7.

3) WIND SPEED VARIATION

To compare the results of using ASFC or traditional SFC during wind variation, the same test performed in case B is done on the MG, Fig. 1. Fig. 17 proves the importance of using the ASFC to have a great effect on the performance of the system compared to the traditional SFC. The controller parameters of ASFC and traditional SFC are written in Table 8.

D. COMPARISON WITH RELATED LITERATURE

For more validation of the proposed ASFC, its application results are compared with those of reference 10, as another published work, when using the system shown in Fig. 18. The system consists of three different loads with ratings illustrated in Table B.3. As reported in Reference 10, the traditional SFC is studied using trial and error to find the values of the PID

TABLE 18. Controller parameters of D-STATCOM.

System Part	Specifications
V_{m_base}	380 V
I_{m_base}	150 A
I_{ss_base}	52.5 A
$\gamma_{vd} = \gamma_{ld}$	1
γ_{pd}	0.5
$T_3 = D_3$	15 ms
$T_4 = D_4$	40 ms
PWM frequency	3000 Hz

TABLE 19. Controller parameters of AC loads.

Induction motor	Linear load	Nonlinear load
0.20 MW, 4.0 poles	$P_{ll} = 1.70$ MW,	$P_{nll} = 0.90$ MW,
138 kV, $X/R = 10$	$Q_{ll} = 0.40$ MVA r	$Q_{nll} = 0.430$ MVA r
$R_{st} = 0.019650$ p.u.		
$L_{st} = 0.03970$ p.u.		
$R_{rt} = 0.019090$ p.u.		
$L_{rt} = 0.03970$ p.u.		

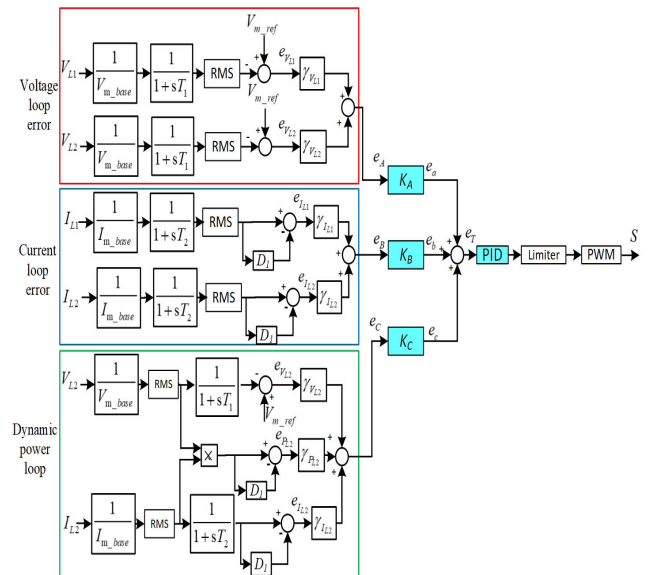


FIGURE 21. The SFC/PID controller circuit.

controller gains (K_p , K_i , and K_d), which is time-consuming. The comparison is carried out on two cases; (i) harmonic analysis and (ii) wind speed variation.

1) HARMONIC ANALYSIS

Fig. 19 shows the THD_v at the PCC for different case studies. It is remarked that the THD_v of the proposed technique is 2%, less than that of the work presented in [10]. The controller parameters of the proposed filter and the SFC controllers are shown in Table 9.

2) WIND SPEED VARIATION

To compare the results of the ASFC with those in [10] during wind variation, it is deemed that the wind speed suddenly rises from 6 to 12 m/s at $t = 0.2$ s and then reduced to

6 m/s at $t = 0.4$ s as shown in Fig. 20 [10]. The results show the importance of using the ASFC-PID controller. It can be noticed that in Figs. 20c,d the active and reactive power consumed at PCC are decreased when using the ASFC controller. The enhancement rate in active power is about 3.5% and that of both reactive power and power factor is about 3%.

V. CONCLUSION

An ASFC compensation scheme using a GOA/PID controller for finding the optimum values of PID gains and minimizing the *ITAE* has been proposed. Different case studies are performed to validate the effectiveness of the proposed ASFC. The simulation results illustrate an improvement of power quality aspects such as dynamic voltage stabilization, mitigation of harmonics distortion, reduction of the consumed reactive power and power factor. The simulation results have been clarified an improvement in the *THD_v* of 94% using the ASFC, while the corresponding improvements using the modified D-STATCOM and the conventional SFC are 50.6% and 80.2%, respectively. For reactive power compensation, the enhancement rate using the ASFC is approximately 4.8%, while for the modified D-STATCOM and conventional SFC are 2.3 % and 4.2 %, respectively. The proposed ASFC can operate on real times as its parameters can be self-tuned to accommodate the present operating conditions. In addition, the optimal minimization of the *ITAE* that speeds up the process is achieved. Furthermore, the D-STATCOM as an alternative device for improving the PQ of the MG is modified to be self-tuned and more effective.

APPENDICES

APPENDIX A

Based on Fig. 21 the following equations are used to calculate the total error from the three loops, e_T , which is the input to the PID controller. The first loop error e_A is obtained as:

$$e_A = \gamma_{V_{L1}} \times (e_{V_{L1}}) + \gamma_{V_{L2}} \times (e_{V_{L2}}) \quad (30)$$

where:

$$e_{V_{L1}} = \frac{V_{m_ref} - V_{L1} \left(\frac{1}{1+sT_1} \right)}{V_{m_base}} \quad (31)$$

$$e_{V_{L2}} = \frac{V_{m_ref} - V_{L2} \left(\frac{1}{1+sT_1} \right)}{V_{m_base}} \quad (32)$$

The second loop error is calculated as follows:

$$e_B = \gamma_{I_{L1}} \times (e_{I_{L1}}) + \gamma_{I_{L2}} \times (e_{I_{L2}}) \quad (33)$$

where:

$$e_{I_{L1}} = \frac{I_{L1}}{I_{m_base}} \left(\frac{1}{1+sT_1} \right) \left(1 - \frac{1}{1+sT_2} \right) \quad (34)$$

$$e_{I_{L2}} = \frac{I_{L2}}{I_{m_base}} \left(\frac{1}{1+sT_1} \right) \left(1 - \frac{1}{1+sT_2} \right) \quad (35)$$

The third loop error is obtained as:

$$e_C = \gamma_{V_{L2}}(e_{V_{L2}}) + \gamma_{I_{L2}}(e_{I_{L2}}) + \gamma_{P_{L2}}(e_{P_{L2}}) \quad (36)$$

where $e_{V_{L2}}$ and $e_{I_{L2}}$ equations are stated in (32) and (35). The term $e_{P_{L2}}$ equation is given in (37):

$$e_{P_{L2}} = \left(\frac{V_{L2}}{V_{m_base}} \times \frac{I_{L2}}{I_{m_base}} \right) \left(1 - \frac{1}{1+sT_2} \right) \quad (37)$$

Therefore, the total error (e_T) is calculated using (38).

$$e_T = e_A + e_B + e_C \quad (38)$$

and

$$e_a = e_A \times K_A \quad (39)$$

$$e_b = e_B \times K_B \quad (40)$$

$$e_c = e_C \times K_C \quad (41)$$

where K_A , K_B , and K_C are selected weightings for the three separate regulation loops to allow control burdens adjustment. It is remarked that the time consumed for simulation processing is more than that of the proposed scheme using ASFC.

APPENDIX B

See Tables 17–19.

REFERENCES

- [1] H. Zou, S. Mao, Y. Wang, F. Zhang, X. Chen, and L. Cheng, "A survey of energy management in interconnected multi-microgrids," *IEEE Access*, vol. 7, pp. 72158–72169, 2019, doi: 10.1109/ACCESS.2019.2920008.
- [2] Q. Liu, Y. Li, L. Luo, Y. Peng, and Y. Cao, "Power quality management of PV power plant with transformer integrated filtering method," *IEEE Trans. Power Del.*, vol. 34, no. 3, pp. 941–949, Jun. 2019, doi: 10.1109/TPWRD.2018.2881991.
- [3] Q. Liu, Y. Li, S. Hu, and L. Luo, "A transformer integrated filtering system for power quality improvement of industrial DC supply system," *IEEE Trans. Ind. Electron.*, vol. 67, no. 5, pp. 3329–3339, May 2020, doi: 10.1109/TIE.2019.2916383.
- [4] M. A. Elshaharty, A. Luna, J. I. Candela, and P. Rodriguez, "A unified power flow controller using a power electronics integrated transformer," *IEEE Trans. Power Del.*, vol. 34, no. 3, pp. 828–839, Jun. 2019, doi: 10.1109/TPWRD.2019.2897601.
- [5] H. Hafezi and R. Faranda, "Dynamic voltage conditioner: A new concept for smart low-voltage distribution systems," *IEEE Trans. Power Electron.*, vol. 33, no. 9, pp. 7582–7590, Sep. 2018, doi: 10.1109/TPEL.2017.2772845.
- [6] A. I. Omar, S. H. E. Abdel Aleem, E. E. A. El-Zahab, M. Algablawy, and Z. M. Ali, "An improved approach for robust control of dynamic voltage restorer and power quality enhancement using grasshopper optimization algorithm," *ISA Trans.*, vol. 95, pp. 110–129, Dec. 2019, doi: 10.1016/j.isatra.2019.05.001.
- [7] O. P. Mahela and A. G. Shaik, "Power quality improvement in distribution network using DSTATCOM with battery energy storage system," *Int. J. Electr. Power Energy Syst.*, vol. 83, pp. 229–240, Dec. 2016, doi: 10.1016/j.ijepes.2016.04.011.
- [8] H. A. Gabbar and A. A. Abdelsalam, "Microgrid energy management in grid-connected and islanding modes based on SVC," *Energy Convers. Manage.*, vol. 86, pp. 964–972, Oct. 2014, doi: 10.1016/j.enconman.2014.06.070.
- [9] A. A. Abdelsalam and A. M. Sharaf, "A novel facts compensation scheme for power quality improvement in wind Smart Grid," in *Proc. 25th IEEE Can. Conf. Electr. Comput. Eng. (CCECE)*, Apr. 2012, pp. 1–4.
- [10] F. H. Gandoman, A. M. Sharaf, S. H. E. Abdel Aleem, and F. Jurado, "Distributed FACTS stabilization scheme for efficient utilization of distributed wind energy systems," *Int. Trans. Electr. Energy Syst.*, vol. 27, no. 11, p. e2391, Nov. 2017, doi: 10.1002/etep.2391.
- [11] M. Talaat, A. Y. Hatata, A. S. Alsayyari, and A. Alblawi, "A smart load management system based on the grasshopper optimization algorithm using the under-frequency load shedding approach," *Energy*, vol. 190, Jan. 2020, Art. no. 116423, doi: 10.1016/j.energy.2019.116423.

- [12] M. Smaoui, A. Abdelkafi, and L. Krichen, "Optimal sizing of stand-alone photovoltaic/wind/hydrogen hybrid system supplying a desalination unit," *Sol. Energy*, vol. 120, pp. 263–276, Oct. 2015, doi: [10.1016/j.solener.2015.07.032](https://doi.org/10.1016/j.solener.2015.07.032).
- [13] A. Elgharbi, D. Mezghani, and A. Mami, "A maximum power point tracking method based on artificial neural network for a PV system," *Int. J. Adv. Eng. Technol.*, vol. 5, no. 1, p. 130, 2012, doi: [10.1016/S1007-0214\(05\)70055-9](https://doi.org/10.1016/S1007-0214(05)70055-9).
- [14] KYOCERA High-Efficiency Photovoltaic Module Datasheet. Accessed: Sep. 23, 2019. [Online]. Available: <https://www.kyocerasolar.com>
- [15] F. A. Farret and M. G. Simoes, *Integration of Alternative Sources of Energy*. Hoboken, NJ, USA: Wiley, 2006.
- [16] M. A. Abdullah, A. H. M. Yatim, C. W. Tan, and R. Saidur, "A review of maximum power point tracking algorithms for wind energy systems," *Renew. Sustain. Energy Rev.*, vol. 16, no. 5, pp. 3220–3227, 2012, doi: [10.1016/j.rser.2012.02.016](https://doi.org/10.1016/j.rser.2012.02.016).
- [17] *Endurance Energy Mfg Ltd*. Accessed: Jul. 1, 2019. [Online]. Available: <https://en.wind-turbine-models.com/manufacturers/247endurance>
- [18] S. Diaf, D. Diaf, M. Belhamel, M. Haddadi, and A. Louche, "A methodology for optimal sizing of autonomous hybrid PV/wind system," *Energy Policy*, vol. 35, no. 11, pp. 5708–5718, Nov. 2007, doi: [10.1016/j.enpol.2007.06.020](https://doi.org/10.1016/j.enpol.2007.06.020).
- [19] I. Baccouche, S. Jemmali, B. Manai, N. Omar, and N. Amara, "Improved OCV model of a li-ion NMC battery for online SOC estimation using the extended Kalman filter," *Energies*, vol. 10, no. 6, p. 764, May 2017, doi: [10.3390/en10060764](https://doi.org/10.3390/en10060764).
- [20] Accessed: Sep. 1, 2020. [Online]. Available: <https://www.rollsbattery.com>
- [21] E. M. Natsheh, A. R. Natsheh, and A. Albarbar, "Intelligent controller for managing power flow within standalone hybrid power systems," *IET Sci., Meas. Technol.*, vol. 7, no. 4, pp. 191–200, Jul. 2013, doi: [10.1049/iet-smt.2013.0011](https://doi.org/10.1049/iet-smt.2013.0011).
- [22] Accessed: Oct. 1, 2020. [Online]. Available: <https://www.powercell.se/>
- [23] *IEEE Recommended Practice and Requirements for Harmonic Control in Electric Power Systems*, IEEE Power and Energy Society, Piscataway, NJ, USA, Standard 519-2014, 2014.
- [24] C. M. Topaz, A. J. Bernoff, S. Logan, and W. Toolson, "A model for rolling swarms of locusts," *Eur. Phys. J. Special Topics*, vol. 157, no. 1, pp. 93–109, Apr. 2008, doi: [10.1140/epjst/e2008-00633-y](https://doi.org/10.1140/epjst/e2008-00633-y).
- [25] T. Jumani, M. Mustafa, M. Rasid, N. Mirjat, M. Baloch, and S. Salisu, "Optimal power flow controller for grid-connected microgrids using grasshopper optimization algorithm," *Electronics*, vol. 8, no. 1, p. 111, Jan. 2019, doi: [10.3390/electronics8010111](https://doi.org/10.3390/electronics8010111).
- [26] S. Li, Y. Li, Y. Cao, Y. Tan, and B. Keune, "Capacity optimisation method of distribution static synchronous compensator considering the risk of voltage sag in high-voltage distribution networks," *IET Gener., Transmiss. Distrib.*, vol. 9, no. 16, pp. 2602–2610, 2015, doi: [10.1049/iet-gtd.2014.1047](https://doi.org/10.1049/iet-gtd.2014.1047).



AHMED HUSSAIN ELMETWALY received the B.Sc. degree from the Higher Institute of Engineering, Elshorouk Academy, Cairo, Egypt, in 2008, and the M.Sc. degree from the Faculty of Engineering, Port Said University, Egypt, in 2015. He is currently an Assistant Teacher with the Department of Electrical Engineering, Higher Institute of Engineering, Elshorouk Academy. His research interests include power quality, smart grids, power system analysis, and renewable energy.

AZZA AHMED ELDESOUKY received the B.Sc. and M.S. degrees in electrical engineering from Suez Canal University, Port Said, Egypt, in 1989 and 1995, respectively, and the Ph.D. degree from Bath University, U.K., in 2002. She is currently working as an Associate Professor with the Department of Electrical Engineering, Port Said University. Her research interests include power system operation and management, power quality, and microgrid stability and control.



ABDELHAY AHMED SALLAM (Life Senior Member, IEEE) received the B.Sc., M.Sc., and Ph.D. degrees from the Faculty of Engineering, Cairo University, Egypt, in 1967, 1972, and 1976, respectively. From 1967 to 1979, he was with the Ministry of Industry. In 1980, he joined the Department of Electrical Engineering, Faculty of Engineering, Suez Canal University, and then Port Said University, Egypt, where he is currently a Professor (Emeritus). He joined Canal Electricity Company as the Head of the Technical Affairs Sector, where he spent four years. In 2006, 2007, 2009, 2012, and 2014, he was a Visiting Professor with the Department of Electrical and Computer Engineering, University of Calgary, Calgary, AB, Canada. He has authored or coauthored over 100 articles in international journals and conferences. He has also authored two books *Electric Distribution Systems* (IEEE-John Wiley & Sons Press, 2011) and *Power System Stability: Modeling, Analysis, and Control* (IET, 2015). His field of interest is mainly power system analysis and planning.

• • •